This article has been accepted for publication in a future issue of this journal, but has not been fully edited. Content may change prior to final publication. Citation information: DOI 10.1109/JSTQE.2019.2911565, IEEE Journal of Selected Topics in Quantum Electronics

STDP-based Unsupervised Spike Pattern Learning in a Photonic Spiking Neural Network with VCSELs and VCSOAs

Shuiying Xiang, Yahui Zhang, Junkai Gong, Xingxing Guo, Lin Lin and Yue Hao

***Abstract*—We propose a photonic spiking neural network (SNN) consisting of photonic spiking neurons based on vertical-cavity surface-emitting lasers (VCSELs). The photonic spike timing dependent plasticity (STDP) is implemented in a vertical-cavity semiconductor optical amplifier (VCSOA). A versatile computational model of the photonic SNN is presented based on the rate equation models. Through numerical simulation, a spike pattern learning and recognition task is performed based on the photonic STDP. The results show that the post-synaptic spike timing (PST) is eventually converged iteratively to the first spike timing (FST) of the input spike pattern via unsupervised learning. Additionally, the convergence rate of the PST can be accelerated for a photonic SNN with more pre-synaptic neurons. The effects of VCSOA parameters on the convergence performance of the unsupervised spike learning are also considered. To the best of our knowledge, such a versatile computational model of photonic SNN for unsupervised learning and recognition of arbitrary spike pattern has not yet been reported, which would contribute one step forward toward numerical implementation of a large-scale energy-efficient photonic SNN, and hence is interesting for neuromorphic photonic systems and spiking information processing.**

***Index Terms*—Photonic spiking neural network, vertical-cavity surface-emitting lasers, vertical-cavity semiconductor optical amplifiers, spike timing dependent plasticity, unsupervised spike pattern learning.**

I. Introduction

SPIKING neural networks (SNNs) are more biologically plausible, hardware friendly and energy-efficient compared with the conventional artificial neural networks[1]. Similar to human brain, the SNN represents input/output data as spikes, but not real-valued vectors. The rate coding and temporal coding are two widely employed schemes in the context of spike encoding [2-6]. For the rate coding, the intensity of stimulus is represented by spiking rate. For the temporal coding, the information is conveyed by the precise timing. Spike timing dependent plasticity (STDP) is believed to be a fundamental synaptic plasticity mechanism in the human brain [7-9]. It describes the modification of synaptic weight based on the precise temporal relations between pre-synaptic and post-synaptic spikes: the synaptic weight is increased whenever a pre-synaptic spike appears prior to a post-synaptic spike, and is decreased otherwise.

Recently, the software-based SNNs have attracted lots of attentions in the field of artificial intelligence. A variety of supervised and unsupervised learning mechanisms have been designed to train the SNNs [10-21]. Besides, significant efforts have also been devoted to the hardware implementations of SNN with electronic neurons and synapses, based on the complementary metal oxide semiconductor (CMOS) technologies or non-volatile memory technologies [22-38] (for more details please refer to Refs. 34 and 35). However, these approaches suffer from different drawbacks in the forms of energy-efficiency and speed.

As an alternative, photonic platform is a promising candidate for hardware implementation of ultrafast brain-inspired computing, due to the fascinating advantages such as high speed, wide bandwidth, and massive parallelism. In recent years, various photonic neurons[39-52], photonic synapses[53-59], as well as photonic neuromorphic systems have been proposed [43, 45-47]. In these photonic neuromorphic systems, vertical-cavity surface-emitting lasers (VCSELs) have been widely employed as the photonic neurons due to the advantages of low power consumption, low cost, and easy implementation of large-scale integration [39, 41, 43, 48-52]. For example, Nahmias et al numerically constructed a simple three-unit spatiotemporal pattern recognition circuit based on excitable VCSELs where a specific pattern corresponding to the fixed coupling delays could be detected [43]. On the other hand, the majority of photonic STDP schemes are realized based on the in-plane semiconductor optical amplifier (SOA). For instance, Fok et al demonstrated supervised learning by using a photonic STDP circuit based on a SOA and an electro-absorption modulator [53]. Ren et al showed that the optical STDP circuit based on two SOAs was able to train a post-synaptic neuron to fire at

Manuscript received Nov 28, 2018. This work is supported in part by the National Natural Science Foundation of China (No.61674119), in part by the Postdoctoral innovation talent program in China (No. BX201600118), in part by the Young Talent fund of University Association for Science and Technology in Shaanxi, China (No.20160109), in part by the project funded by China Postdoctoral Science Foundation (No.2017M613072), in part by Natural Science Basic Research Plan in Shaanxi Province of China(No.2017JM6002, 2016JM6009).

S. Xiang is with State Key Laboratory of Integrated Service Networks, Xidian University, Xi'an 710071, China; and also with State Key Discipline Laboratory of Wide Bandgap Semiconductor Technology, School of Microelectronics, Xidian University, Xi'an 710071, China (email: jxxsy@126.com).

Y. Zhang, J. Gong, X. Guo, L. Lin are with State Key Laboratory of Integrated Service Networks, Xidian University, Xi'an 710071, China.

Y. Hao is with State Key Discipline Laboratory of Wide Bandgap Semiconductor Technology, School of Microelectronics, Xidian University, Xi'an 710071, China

This article has been accepted for publication in a future issue of this journal, but has not been fully edited. Content may change prior to final publication. Citation information: DOI 10.1109/JSTQE.2019.2911565, IEEE Journal of Selected Topics in Quantum Electronics

specific time through reinforcement learning [55]. Toole et al experimentally demonstrated a photonic STDP module towards supervised learning and unsupervised pattern recognition based on a single SOA [57]. In these reported photonic STDP circuits, the operating current of SOA is usually large, i.e., several tens of or hundreds of mA, which is undesirable for low power consumption neuromorphic computing applications. Actually, when operating below threshold, the VCSEL can serve as a Fabry–Pérot (FP) amplifier, and is also referred to as a vertical-cavity semiconductor optical amplifier (VCSOA) [60-62]. In our previous work, we predicted that the VCSOA could provide a feasible low-power solution for photonic STDP and could be easily integrated with the VCSEL-based photonic spiking neuron[63]. However, the photonic STDP based on the VCSOA has not yet been incorporated into a photonic SNN for unsupervised learning. Additionally, the previously reported photonic spike pattern recognition circuits are limited to detect specific patterns, but are unable to detect arbitrary temporal spike patterns. In particular, a versatile computational model which is highly desirable for designing large-scale photonic SNN has not yet been addressed.

In this paper, we propose to design a photonic SNN with VCSELs and VCSOAs to implement arbitrary spike patterns recognition. The main contributions: first, a versatile computational model of photonic SNN is derived for the first time. Second, unsupervised spike pattern learning and recognition is realized based on photonic STDP which is implemented in a VCSOA. Third, we further examine the effects of bias current of VCSOA and initial wavelength detuning on the convergence performance of unsupervised spike learning. The rest of this paper is organized as follows. In Section II, the system architecture of the proposed photonic SNN is described. In addition, the theoretical models of photonic spiking neuron based on VCSEL and photonic STDP based on VCSOA are presented. In Section III, the temporal spike encoding and the photonic STDP rule are described. The performances of the unsupervised spike pattern leaning and recognition task are examined. Finally, conclusions are drawn in Section IV.

II. THEORYAND MODEL

A. Architecture of the proposed photonic SNN

The schematic diagram of a photonic SNN based on VCSELs and VCSOAs is presented in Fig.1. The photonic SNN consists of n VCSELs as pre-synaptic neurons and one VCSEL as a post-synaptic neuron. The pre-synaptic neurons and post-synaptic neuron are connected via adaptive synapses that are capable of performing photonic STDP. Here, the synapses comprise the variable synaptic weight devices (Wi) and the STDP array. The STDP array is the same as the photonic STDP circuit based on a VCSOA presented in our previous work [63]. The photonic SNN can be divided into three functional parts: the encoding part, the learning part and the readout part. In the encoding part, the external input pulses (stimuli) are encoded into spikes with different spike timing by the pre-synaptic VCSELs. In the learning phase, the STDP rule accomplished by

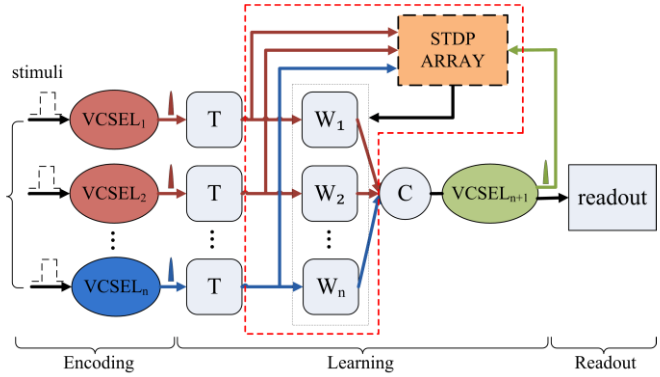

Fig. 1. Schematic diagram of photonic SNN based on VCSELs and VCSOAs. n photonic presynaptic neurons and one postsynaptic neuron are conneted with optical STDP synapses. $VCSEL_1$-$VCSEL_n$: photonic presynaptic neurons; $VCSEL_{n+1}$: photonic postsynaptic neuron; T: variable delay line; W_i(i=1,2,…,n): variable synaptic weight device connecting $VCSEL_i$ and $VCSEL_{n+1}$; STDP ARRAY: optical STDP synapses realized by VCSOAs; C: optical coupler. The red dashed box represents the ex-situ approach for updating the synaptic weight.

the VCSOA is utilized to update the synaptic weight. Here, only the ex-situ approach is considered for the unsupervised learning in the photonic SNN, which is similar to Ref. [57]. More precisely, in a possible experiment, the STDP curve can be measured at the level of single synapse in advance [63]. Then, for each learning cycle, the amount of weight change ($\Delta\omega$) between any pair of pre-synaptic and post-synaptic spikes can be calculated by external circuit or computer according to the photonic STDP rule [57], the modified weight is finally imported to the hardware. The aim of the readout part is to recognize the spike pattern from the response of post-synaptic neuron. Note that, all of the spikes generated by the pre-synaptic neurons propagate to the post-synaptic neuron and are temporally accumulated by the post-synaptic neuron. If the integral value exceeds the excitability threshold, an output spike will be formed (spike in green). During the learning procedure, the post-synaptic spike timing (PST) will be quite different at each learning cycle. Here, we use the PST after convergence as the identification of a given spike pattern.

B. Model of photonic neuron: rate equations of VCSEL

The VCSEL with an embedded saturable absorber (VCSEL-SA) is employed here to mimic a leaky integrate-and-fire neuron. The rate equations of a VCSEL-SA subjected to incoherent external input pulse injection are written as follows [43, 50]:

$$\frac{dS_i}{dt} = \Gamma_a g_a(n_{ia} - n_{0ia})S_i + \Gamma_s g_s(n_{is} - n_{0is})S_i - \frac{S_i}{\tau_{ph}} + \beta B_r n_{ia}^2 \tag{1}$$

$$\frac{dn_{is}}{dt} = -\Gamma_s g_s(n_{is} - n_{0is})S_i - \frac{n_{is}}{\tau_s} + \frac{I_s}{eV_s} \tag{2}$$

$$\frac{dn_{ia}}{dt} = -\Gamma_a g_a(n_{ia} - n_{0ia})[S_i - k_e \frac{\tau_{ph}}{hc/\lambda_e}\frac{P_e(t,\Delta\tau)}{V_a}] - \frac{n_{ia}}{\tau_a} + \frac{I_a}{eV_a} \tag{3}$$

Table 1. VCSEL-SA Parameters [43, 50]

Param.	Gain region	Absorber region
Cavity volume $V_{a,s}$	$2.4\times10^{-18}\,\mathrm{m}^3$	$2.4\times10^{-18}\,\mathrm{m}^3$
Confinement factor $\Gamma_{a,s}$	0.06	0.05
Carrier lifetime $\tau_{a,s}$	1 ns	100 ps
Differential gain/loss $g_{a,s}$	$2.9\times10^{-12}\ \mathrm{m^3s^{-1}}$	$14.5\times10^{-12}\ \mathrm{m^3s^{-1}}$
Transparency carrier density $n_{0a,s}$	$1.1\times10^{24}\ \mathrm{m^{-3}}$	$0.89\times10^{24}\ \mathrm{m^{-3}}$

Where the subscript i ($i=1,2,...,n$) denotes the serial number of pre-synaptic neurons. The subscripts a and s stand for the gain and absorber regions, respectively. $S_i(t)$ represents the photon density in the cavity, $n_a(t)$ ($n_s(t)$) is the carrier density in the gain (absorber) region. The term $k_e\tau_{ph}/(hc/\lambda_e)P_e(t,\Delta\tau)/V_a$ in Eq. (3) denotes the external input optical pulse, and k_e ($\Delta\tau$) is the input strength (temporal duration). For simplicity, we consider $P_e=1\mathrm{mW}$, $\lambda_e=845.58\mathrm{nm}$. The output power of pre-synaptic VCSELs can be expressed as $P_i(t)\approx\eta_c\Gamma_a S_i(t)V_a\,hc/(\tau_{ph}\lambda_i)$ [43, 50]. Other parameters are the bias current in the gain (absorber) region I_a (I_s), the wavelength of VCSELs λ_i (845.58nm), the speed of light c, the spontaneous emission coupling factor β, the bimolecular recombination term B_r, the output power coupling coefficient η_c, and the photon lifetime τ_{ph}.

For the post-synaptic neuron, the Eq. (3) should be replaced as follows [43, 50],

$$\frac{dn_{oa}}{dt}=-\Gamma_a g_a(n_{oa}-n_{0oa})(S_o-\sum_{i=1}^{n}\omega_i\frac{\tau_{ph}}{hc/\lambda_i}\frac{P_i(t-T)}{V_a}) -\frac{n_{oa}}{\tau_a}+\frac{I_a}{eV_a} \tag{4}$$

Where the subscript o denotes the post-synaptic neuron. The term $\sum_{i=1}^{n}\omega_i\frac{\tau_{ph}}{hc/\lambda_i}\frac{P_i(t-T)}{V_a}$ represents inputs of the post-synaptic neuron, which are exactly the weighted sum of all the pre-synaptic neurons with transmission delay $T=3\mathrm{ns}$. ω_i is the coupling strength, which is the physical variable associated with the synaptic weight in the photonic SNN that needs to be adjusted according to the STDP rule. The rest equations and parameters are the same as those for the pre-synaptic neurons. In simulation, we use typical parameters for the VCSELs-SA [43, 50]: $I_s=0\mathrm{mA}$, $h=6.63\times10^{-34}\,\mathrm{J\cdot s}$, $B_r=10\times10^{-16}\,\mathrm{m^3s^{-1}}$, $\beta=1\times10^{-4}$, $\eta_c=0.4$, $\tau_{ph}=4.8\times10^{-12}$ s. The other device parameters are considered to be identical for all the VCSELs-SA and are summarized in Table 1.

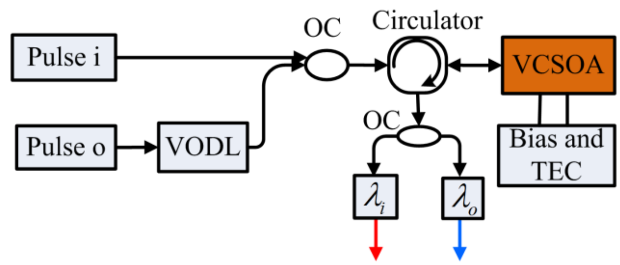

Fig. 2. Schematic diagram of photonic STDP based on VCSOA. Pulse i and Pulse o represent the optical pulse injection beams; VODL is the variable optical delay line, OC is the optical coupler; Circulator is the optical circulator; VCSOA is the vertical-cavity semiconductor optical amplifier; Bias and TEC is the bias current and temperature controller for the VCSOA; $\lambda_{i,o}$ in the box means a bandpass filter.

C. Model of photonic STDP: rate equations of VCSOA

The schematic diagram of photonic STDP based on a VCSOA is presented in Fig. 2, where the pulse i and pulse o can be generated by the pre-synaptic and post-synaptic neurons, respectively. The difference of relative time delay between two injection beams can be controlled by a VODL, and is defined as $\Delta t=t_o-t_i$, where $t_{i,o}$ denote the peak location of two optical pulses. The detailed calculation of $\Delta\omega$, i.e., the amount of weight change for a given Δt, has been presented in our previous work[63].

The most two popular methods to numerically study the VCSOAs are rate equation approach and FP approach [64-67]. For a VCSOA subject to two injection pulse beams, the FP approach can be written as follows [61, 62]:

$$\frac{dN}{dt}=\frac{\eta I}{e\Gamma_1 V}-(AN+BN^2+CN^3) -\frac{\Gamma c\xi a(N-N_0)}{n_c}(\beta_{sp}\bar{S}_{ase}+\bar{S}_i+\bar{S}_o) \tag{5}$$

$$\bar{S}_{ase}=\left(\frac{(G_s-1)[(1-R_b)(1+R_tG_s)+(1-R_t)(1+R_bG_s)]}{gL_c(1-R_tR_be^{2gL_c})}-2\right)\frac{\Gamma_1 BN^2 n_c}{gc} \tag{6}$$

$$\bar{S}_{i,o}=\left(\frac{(1-R_t)(1+R_bG_s)(G_s-1)}{(1-\sqrt{R_tR_b}G_s)^2+4\sqrt{R_tR_b}G_s\sin^2\Phi_{i,o}}\right)\frac{P_{i,o}n_c\lambda_p}{hc^2Vg} \tag{7}$$

where N is the carrier density, $\bar{S}_{ase}$ is the averaged spontaneous photon density. $\bar{S}_{i,o}$ represent the averaged stimulated photonic density related to the dual optical pulse injection beams, respectively. I is the bias current of VCSOA. The term $G_s=e^{gL_c}$ denotes the single-pass gain, and $g=\Gamma\Gamma_1\xi a(N-N_0)-\alpha_i$. The single-pass phase change can be described as [61, 62]:

$$\Phi_{i,o}=\Phi_{0i,0o}-b\Gamma\Gamma_1\xi L_c a(N-N_s)/2 \tag{8}$$

where $\Phi_{0i,0o}=2\pi n_c L_c(1/\lambda_{i,o}-1/\lambda_p)$ represent the initial phase detuning, λ_p=845.58nm is the peak resonant wavelength of the VCSOA, and $\lambda_{i,o}$ denote wavelengths of optical pulse injection beams. The second term in Eq. (8) couples the optical phase to the carrier density in the amplifier. N_s denotes the carrier density for the VCSOA without optical pulse injection. The initial wavelength detuning is introduced as $\Delta\lambda_{i,o}=\lambda_{i,o}-\lambda_p$.

This article has been accepted for publication in a future issue of this journal, but has not been fully edited. Content may change prior to final publication. Citation information: DOI 10.1109/JSTQE.2019.2911565, IEEE Journal of Selected Topics in Quantum Electronics

Table 2. Some typical parameters of VCSOA used in simulation [61, 62].

Param.	Description	Value
R_t	Top DBR reflectivity	0.99
R_b	Bottom DBR reflectivity	0.9995
n_c	Cavity refractive index	3.3
V	Cavity volume	$3.86\times10^{-17}\mathrm{m}^3$
L_c	Effective cavity length	$3\lambda_p / n_c$
b	Linewidth enhancement factor	2.7
a	Linear material gain coefficient	$2.48\times10^{-20}\mathrm{m}^2$
α_i	Average cavity loss coefficient	$1165\mathrm{m}^{-1}$
ξ	Gain enhancement factor	1
η	Internal quantum efficiency	0.4
Γ	Lateral confinement factor	1
Γ_1	Longitudinal confinement factor	0.1
A	Nonradiative recombination rate	$1\times10^{8}s^{-1}$
B	Radiative recombination coefficient	$1\times10^{-16}\mathrm{m}^6s^{-1}$
C	Auger recombination coefficient	$5\times10^{-42}\mathrm{m}^6s^{-1}$
N_0	Transparency carrier density	$2\times10^{24}\mathrm{m}^{-3}$
β_{sp}	Spontaneous emission factor	2.5×10^{-5}

$P_{i,o}$ are the optical power of two optical pulse injection beams, respectively. The other parameters are defined in Table 2. With these parameters, the threshold current of VCSOA is about 6.1mA [61].

The amplifier gain for a VCSOA operating in reflection mode can be described as [62, 64]:

$$G_{Ri,Ro}=\frac{(\sqrt{R_t}-\sqrt{R_b}G_s)^2+4\sqrt{R_tR_b}G_s\sin^2\Phi_{i,o}}{(1-\sqrt{R_tR_b}G_s)^2+4\sqrt{R_tR_b}G_s\sin^2\Phi_{i,o}} \quad (9)$$

Then the output power can be calculated by $P_{outi,outo}=P_{i,o}G_{Ri,Ro}$.

III. Numerical Results

In this section, we firstly consider the temporal spike encoding based on the VCSEL. Then the photonic STDP learning rule based on the VCSOA is presented. At last, the performance of unsupervised spike pattern learning and recognition based on the photonic SNN is examined numerically.

A. Temporal spike encoding based on VCSEL

We numerically solve the rate equations using fourth-order Runge-Kutta method. The calculated threshold current is about I_{th}=2.4mA for a solitary VCSEL. The injection current of VCSEL is set as I_a=2mA.

Here, we consider three cases of external input rectangular pulse for $\Delta\tau=0.45$ns. The center timings of the pulse are fixed at $t_c=9.75$, 10 and 10.25ns, respectively. Note that, one can encode external stimuli into different numbers of spikes by

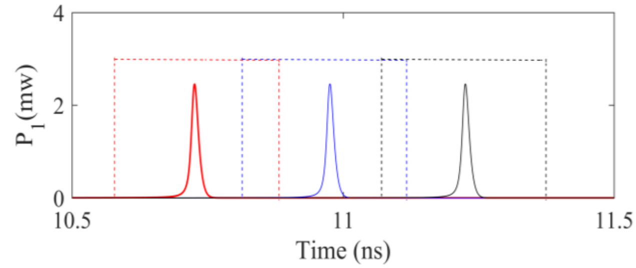

Fig. 3. External input rectangular pulse (dashed line) and corresponding spike outputs (solid line) of VCSEL-based photonic neuron.

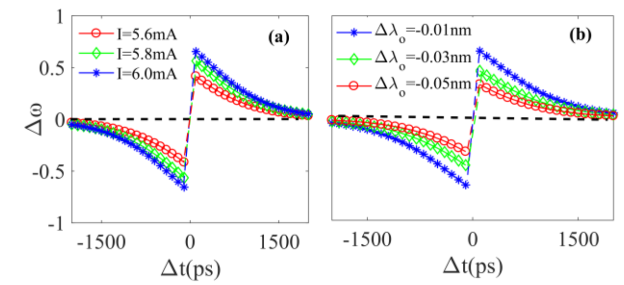

Fig. 4. The photonic STDP curves for (a) I =5.6mA, 5.8mA and 6mA, with $\Delta\lambda_o$=-0.01nm , (b) $\Delta\lambda_o$ =-0.05nm, -0.03nm and -0.01nm, with I=6mA . The black dashed line corresponds to $\Delta\omega=0$.

changing k_e [50]. For simplicity, only the single spike output is considered here. The outputs of the VCSELs-based neurons are presented in Fig. 3 for $k_e=1.0$. Obviously, the rectangular pulse is encoded into spike, and each VCSEL-based pre-synaptic neuron fires only once within the encoding window. These pre-synaptic spikes at various timings form an input spike pattern.

B. Photonic STDP based on VCSOA

The calculated STDP curves for different I and $\Delta\lambda_o$ are shown in Fig. 4. Here, $\Delta\omega$ is the amount of weight change for a given Δt. It can be seen that, the STDP curve closely resembles the STDP response in a biological neuron, and is similar to the experimental measurement for the conventional SOA [53, 55, 57-58]. Note, the learning window of the photonic STDP based on the VCSOA is much wider than that for the conventional SOA [55, 68], which can be attributed to the fact that the gain recovery time of VCSOA is longer than that of conventional SOA [55, 68]. Note, such longer recovery time may be associated with the small bias current as well as the resonant nature of the VCSOA, which finally determines the temporal resolution of the unsupervised spike learning algorithm based on STDP. Besides, on the one hand, for a given wavelength detuning $\Delta\lambda_o=-0.01$nm, a larger (smaller) I leads to increased (decreased) height and increased (decreased) width of the STDP curves. Moreover, the bias current of a VCSOA is much smaller than that of a conventional SOA, which leads to much lower power consumption. On the other hand, for a given bias current $I=6$mA, a larger (smaller) $|\Delta\lambda_o|$ leads to decreased (increased) height and decreased (increased) width of the STDP curves. Hence, it is suggested to set the input wavelength to be close to the cavity resonant wavelength to obtain high gain [66]. It has been demonstrated that, the maximum

This article has been accepted for publication in a future issue of this journal, but has not been fully edited. Content may change prior to final publication. Citation information: DOI 10.1109/JSTQE.2019.2911565, IEEE Journal of Selected Topics in Quantum Electronics

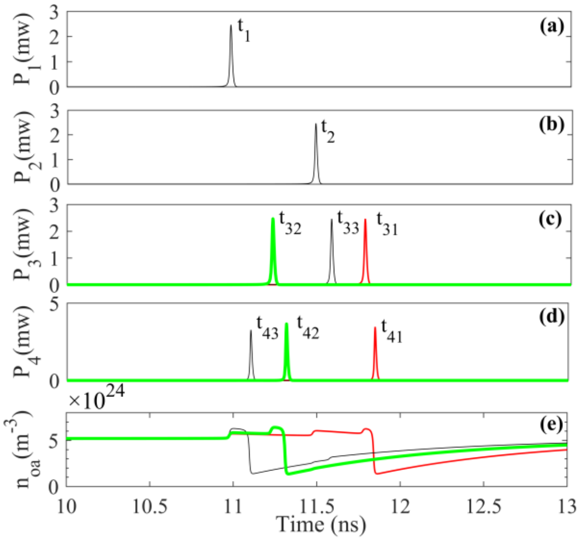

Fig. 5. Input spike pattern generated by pre-synaptic VCSELs and the output spike generated by the post-synaptic VCSEL. (a) The spike encoded by $VCSEL_1$ at fixed timing t_1, (b) the spike encoded by $VCSEL_2$ at fixed timing t_2, (c) the spikes encoded by $VCSEL_3$ at random fire timing, (d) the output spikes of the post-synaptic $VCSEL_4$ during the learning process, (e) n_{oa} of the post-synaptic $VCSEL_4$ during the learning process.

optical bandwidth can reach 100GHz (0.6nm) by optimizing the operating conditions [69]. Here, the input wavelengths are set as $\Delta\lambda_i$ =845.58nm and $\Delta\lambda_o$ =845.57nm, respectively, and the bias current of VCSOA is fixed at 6mA, unless otherwise stated.

In this work, the photonic STDP curve is calculated in advance. Then, the $\Delta\omega(\Delta t)$ is stored and could be used to update the synaptic weight through an ex-situ learning approach.

During the learning phase, the modification of synaptic weight from learning cycle x to $x+1$ is computed as follows [11]:

$$\omega_i(x+1) = \omega_i(x) + \omega_f \times \Delta\omega(\Delta t) \tag{8}$$

where $\omega_i(x)$ and $\omega_i(x+1)$ are the weights of synapse i at $x-th$ and $(x+1)-th$ learning cycles, respectively. ω_f stands for the learning rate, and is 0.01 in this paper, unless otherwise stated.

C. Spike pattern learning and recognition based on photonic SNN

In the following, the performance of spike pattern learning and recognition based on the proposed photonic SNN is examined. In simulation, the post-synaptic neuron is set to be below threshold initially, and the initial synaptic weights should be properly selected to successfully trigger a post-synaptic spike. We also consider the noise which may be originated from different background in practice by introducing pre-synaptic random neurons with random spike timing (spike in blue in Fig.1). The time duration of each learning cycle is 20ns. For each cycle, the input spike pattern is repeated and the random background noise is also added. For the pre-synaptic neurons firing at fixed timings, we suppose that the spike timings are in an increasing order, i.e., $t_i < t_j$ if $i < j$.

For simplicity, we firstly consider a simple photonic SNN with n=3. Namely, there are three pre-synaptic neurons and one post-synaptic neuron. Here, the initial weights of three photonic synapses are all set to be 1.75. The input spike patterns and output spikes at some representative learning cycles are shown in Fig. 5. Note that, for the purpose of direct comparison, the x-axes for the Figs. 5(d) and (e) are shifted to left by 3ns to compensate the transmission delay T. As shown in Figs.5 (a) and (b), t_1 and t_2 (with $t_1 < t_2$), which represent the input spike pattern, are fixed during the entire learning process. For convenience, we denote t_1 as the first spike timing (FST) of the input spike pattern. We consider that t_3 denoting the background noise follows a uniform distribution (9.8ns, 10.8ns). As shown in Fig.5(c), t_{31} (t_{33}) is the fire timing at the beginning (after convergence) of the learning, t_{32} denotes the fire timing during the learning process. Correspondingly, t_{41}, t_{42}, t_{43} shown in Fig.5 (d) are the PST values. As shown in Fig.5 (e), at the beginning of the learning process, the carrier density exceeds the excitability threshold when the post-synaptic neuron receives all the three pre-synaptic spikes at t_1, t_2 and t_{31}, leading to a post-synaptic spike at t_{41} in Fig.5(d). The post-synaptic spike at t_{42} is generated when the post-synaptic neuron receives two pre-synaptic spikes at t_1 and t_{32}. After the convergence of the learning, post-synaptic neuron reaches its excitability threshold just after it receives the first pre-synaptic spike, and fires at t_{43}. As can be clearly observed in Fig. 5 (d), $t_{41} > t_{42} > t_{43}$, indicating that the PST is decreased during the learning procedure. Moreover, we find that t_{43} is close to t_1, indicating that the PST stabilizes at the FST after convergence.

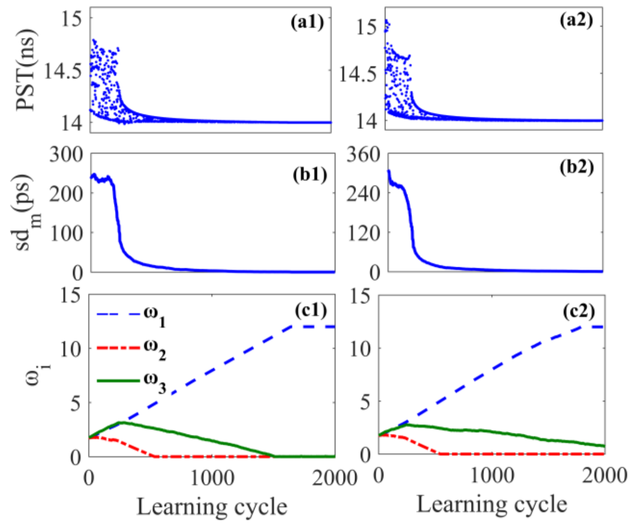

Fig. 6. (a1, b1) PST, (a2, b2) standard deviation of PST, (a3, b3) Synaptic weights for t_3 following uniform distribution (9.8ns, 10.8ns) (left column) and (9.5ns, 11.0ns) (right column).

To present more insight into the evolution of learning process, we further consider the PST at each learning cycle. In order to quantify the performance of convergence for unsupervised learning, we further calculate the standard deviation of the PST. For convenience, we consider that the learning process is converged if the standard deviation of the PST remains within $4ps$ for 100 consecutive learning cycles. The convergence cycle is denoted as the first of these 100 cycles. Mathematically, the defined standard deviation of PST is calculated by

This article has been accepted for publication in a future issue of this journal, but has not been fully edited. Content may change prior to final publication. Citation information: DOI 10.1109/JSTQE.2019.2911565, IEEE Journal of Selected Topics in Quantum Electronics

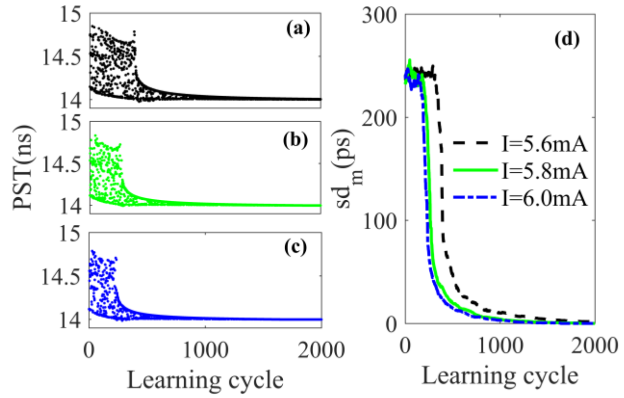

Fig. 7. PST (left column) and sd_m (right) for different I, (a) with $I = 5.6\text{mA}$, (b) with $I = 5.8\text{mA}$, (c) with $I = 6.0\text{mA}$.

$sd_m = \sqrt{\sum_m^{m+100}(t_{4m} - t_{mean})^2/100}$, where the subscript m represents the first cycle of the 100 consecutive cycles, t_{4m} represents the corresponding spike timing, and t_{mean} is the mean PST of the 100 consecutive cycles. Note that, in practice, when the convergence criterion is satisfied, no further learning cycle is needed.

The PST values and the corresponding standard deviations are presented in Figs.6 (a1) and (a2). It can be observed from Fig.6 (a1) that, the PST distributes widely in the range from 14.1ns to14.8ns at the beginning, and sd_m=250ps. After learning about 250 cycles, the distribution of PST becomes much narrower, and sd_m decreases substantially. At about 890-th cycle, the PST is almost constant and is close to t_1. Additionally, our defined convergence criterion, i.e. $sd_m < 4\text{ps}$, is also satisfied. That is to say, in a completely unsupervised manner, the post-synaptic neuron can find the FST of a given input spike pattern, which is similar to findings obtained in Ref. [14]. The three synaptic weights are further presented in Fig. 6(a3). It can be seen that, ω_1 increases firstly until reaches its maximum and then keeps unchanged, ω_2 fluctuates firstly and then decreases until to 0, ω_3 increases firstly and then decreases with fluctuation due to the random distribution of t_3. Without loss of generality, we also consider one case for which t_3 follows uniform distribution (9.5ns, 11.0ns). As presented in Figs. 6(b1) - (b3), the overall trend is hardly affected by the noise distribution, but the convergence cycle is m=1059. Namely, more learning cycles are required to meet the convergence criterion due to the wider distribution of t_3. Note, we have also considered some other initial synaptic weights, and obtain similar results with slightly different convergence cycles.

Next, we explore the effects of the VCSOA parameters on the convergence performance of the unsupervised spike learning. The effects of different I and $\Delta\lambda_o$ are considered. The PST values are presented in Figs. 7(a)-(c) for I =5.6mA, 5.8mA and 6.0mA, respectively. It can be seen from Fig. 7(d) that, the convergence cycles are m=892, 1016 and 1478 for I =6.0mA, 5.8mA and 5.6mA, respectively. Namely, more learning cycles are required to meet the convergence criterion for smaller I

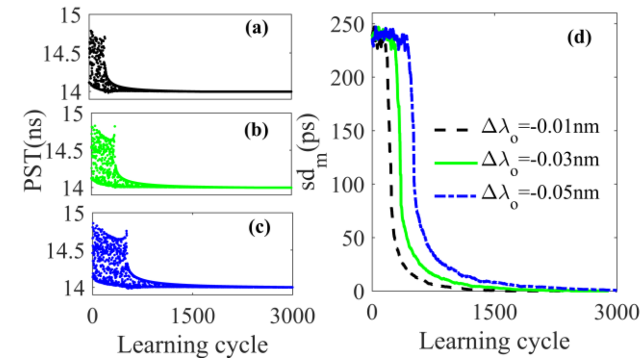

Fig. 8. PST (left column) and sd_m (right) for different $\Delta\lambda_o$, (a) with $\Delta\lambda_o = -0.01\text{nm}$, (b) with $\Delta\lambda_o = -0.03\text{nm}$, (c) with $\Delta\lambda_o = -0.05\text{nm}$.

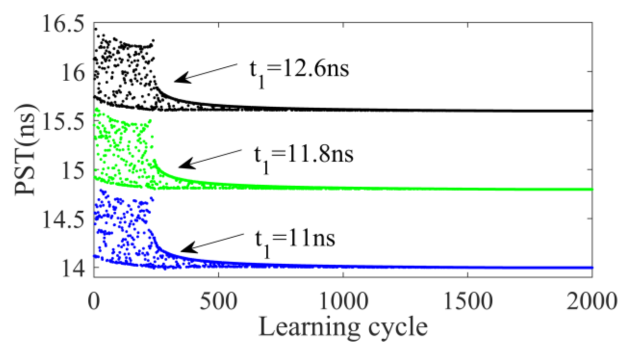

Fig. 9. PST for three arbitrary spike patterns with different FST.

due to the small height of STDP curve. Better convergence performance can be achieved for a higher bias current. Hence, a proper bias current should be selected according to the trade-off between the convergence performance and power consumption.

Similarly, the PST values and the corresponding standard deviations for different $\Delta\lambda_o$ are presented in Fig.8. It can be seen that, a smaller $|\Delta\lambda_o|$ leads to a smaller learning cycle at which the PST values converge to the FSL of input pattern, which can be attributed to the fact that the FP-like VCSOA is sensitive to wavelength detuning. Hence, it is suggested to adjust the input wavelength to be close to the cavity resonant wavelength to obtain better convergence performance.

Next, we consider several arbitrary spike pattern recognition tasks which are represented by different FST of input spike patterns. The distributions of PST for three representative cases are presented in Fig.9. It is found that, the evolution trends of PST are similar for all the three cases. After convergence, the PST values converge to their corresponding FST for a given task. As a consequence, different spike patterns can be recognized successfully in an unsupervised fashion based on the photonic SNN according to the photonic STDP rule.

In practice, the external noise may change the encoded spike patterns. Hence, it is highly desirable to exmine the robustness to noise. To this end, we add some jitters to the spike patterns [11, 14], and test whether the PST will be convergent. According to Fig. 10, the PST will tend to converge for the conditions of jitter = 2ps and jitter = 5ps. However, for the case of jitter = 20ps, the convergence criterion identified previously is not satisfied. That is to say, the photonic STDP-based learning rule is robust to noise to some extent.

This article has been accepted for publication in a future issue of this journal, but has not been fully edited. Content may change prior to final publication. Citation information: DOI 10.1109/JSTQE.2019.2911565, IEEE Journal of Selected Topics in Quantum Electronics

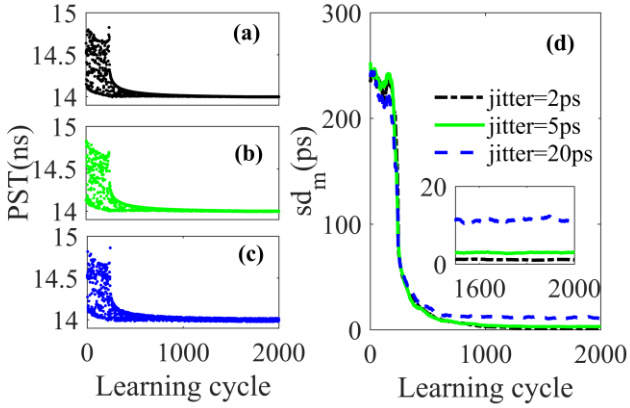

Fig. 10. PST (left column) and sd_m (right) for different jitters, (a) with jitter=2ps, (b) with jitter=5ps, (c) with jitter=20ps.

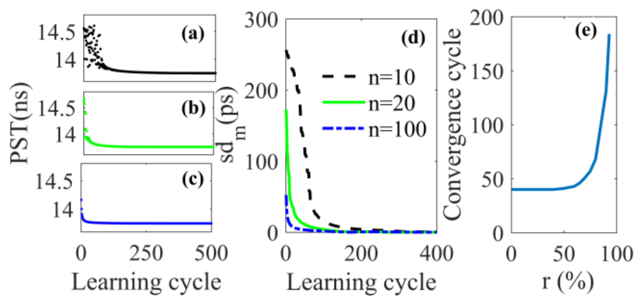

Fig. 11. PST (left column) and sd_m (middle column) for different n. (a) with $n=10$, (b) with $n=20$, (c) with $n=100$. (e) Convergence cycle as a function of ratio of pre-synaptic random neurons, with n=100.

Subsequently, we also perform the simulations for other cases of learning rate (not shown here). The convergence cycles corresponding to $sd_m < 4ps$ are $m = 434$ for ω_f=0.02, $m = 105$ for ω_f=0.01, and $m = 51$ for ω_f=0.2, respectively. That is to say, for a larger ω_f, the PST values converge to the FST of input pattern at a smaller learning cycle. But note that, a smaller ω_f could ensure a more robust learning [14].

At last, we consider the spike pattern recognition in a larger photonic SNN with more pre-synaptic neurons. The PST values and the sd_m are depicted in Fig. 11 for three cases of n. For convenience, for each case of n, the number of the fixed pre-synaptic neurons is assumed to be equal to that of the random pre-synaptic neurons. The initial weights for all the synapses are set as 0.3, 0.225, and 0.05 for n=10, n=20, and n=100, respectively. The learning rate is fixed at ω_f=0.01. It can be seen that, the PST values decrease more sharply for a large n. Besides, the convergence criterion can be satisfied for all the cases of n. More precisely, the convergence cycles corresponding to $sd_m < 4ps$ are $m = 199$ for n=10, $m = 99$ for n=20, and $m = 41$ for n=100, respectively. Namely, for the same learning rate, less learning cycles are needed to reach the convergence criterion for a larger n. Nevertheless, we find that the convergence rate will be saturated for further increase of n(not shown here). Thus, the convergence rate can be improved for a photonic SNN with more pre-synaptic neurons.

Without loss of generality, the photonic SNN with different numbers of pre-synaptic random neurons are also considered. Here, the ratio of pre-synaptic random neurons is defined as r = number of random neurons$/n$. The convergence cycle as a function of r is further presented in Fig. 11(e) for n=100. It can be seen that, the post-synaptic neuron could successfully recognize the input pattern at about $m \approx 41$ ($m \le 50$) for $r \le 50\%$ ($r \le 70\%$). But when $r > 70\%$, the convergence cycle increases sharply, indicating that the post-synaptic neuron needs more cycle to learn and recognize the patterns, or the learning process could never converge.

Note that, in the present study, only one spike pattern can be recognized at a time by the single post-synaptic neuron, in order to simultaneously achieve multiple spike patterns recognition, the photonic SNN with multiple post-synaptic neurons and lateral inhibition mechanism may be required [15]. By combining the inhibitory dynamics of photonic neuron [70, 71], multiple spike patterns recognition will be performed in the near future. In addition, the present work is limited to the ex-situ learning method for the photonic SNN. As an alternative, designing an in-situ learning approach for the photonic SNN, which may still be exceptionally challenging and demanding, can take full advantages of speed and energy for the photonics platforms [72], and thus also deserves additional innovations.

IV. Conclusion

In summary, we proposed to design a photonic SNN consisting of VCSEL-based photonic spiking neurons, in which the photonic STDP is implemented in a VCSOA. A versatile computational model was constructed based on the rate equation models. By numerical simulation, a cluster task, with respect to recognize the FST of an arbitrary spike pattern, was accomplished in the proposed photonic SNN. In particular, the learning is performed according to the photonic STDP rule in an unsupervised manner. Besides, we found that better convergence performance can be achieved for a larger bias current of VCSOA and for smaller initial wavelength detuning. Furthermore, the convergence rate of the spike pattern recognition based on photonic SNN could be enhanced by using photonic SNN with more pre-synaptic neurons.

To the best of our knowledge, such photonic SNN consisting of VCSELs and VCSOAs has not yet been reported, which bridges the gap between the isolated computing devices and the photonic SNN. Moreover, this is the first work in which an arbitrary spike pattern can be recognized in an unsupervised manner in a photonic SNN. Note that, VCSELs and VCSOAs are easier to be integrated and are lower power consumption compared with the traditional counterparts, which shows promise in realizing large-scale energy-efficient photonic SNN. Furthermore, the versatile computational model guarantees numerical implementation of a large-scale photonic SNN, and is expected to provide theoretical guideline for the ultrafast photonic neuromorphic systems and brain-inspired photonic information processing.

Acknowledgment

The authors would like to thank Dr. T. Masquelier at the National Center for Scientific Research (CNRS) for helpful discussions.

This article has been accepted for publication in a future issue of this journal, but has not been fully edited. Content may change prior to final publication. Citation information: DOI 10.1109/JSTQE.2019.2911565, IEEE Journal of Selected Topics in Quantum Electronics

REFERENCES

[1] W. Maass, "Networks of spiking neurons: The third generation of neural network models," *Neural Netw.*, vol. 10, no. 9, pp. 1659-1671, Dec. 1997.

[2] Z. F. Mainen, and T. J. Sejnowski, "Reliability of spike timing in neocortical neurons," *Science*, vol. 268, no. 5216, pp.1503–1506, Jul.1995.

[3] J. Gautrais and S. Thorpe, "Rate coding versus temporal order coding: A theoretical approach," *Biosystems*, vol. 48, no. 1-3, pp. 57–65, 1998.

[4] S. Thorpe, A. Delorme, and R. Van Rullen, "Spike-based strategies for rapid processing," *Neural Netw*., vol. 14, no. 6-7, pp. 715-725, Jul. 2001.

[5] E. M. Izhikevich, "Simple model of spiking neurons," *IEEE Trans. Neural Netw.*, vol. 14, no. 6, pp. 1569-1572, Nov. 2003.

[6] T. Gollisch and M. Meister, "Rapid neural coding in the retina with relative spike latencies," *Science*, vol. 319, no. 5866, pp. 1108-1111, Feb. 2008.

[7] G. Bi and M. Poo, "Synaptic modifications in cultured hippocampal neurons: Dependence on spike timing, synaptic strength, and postsynaptic cell type," *J. Neurosci.*, vol. 18, no. 24, pp. 10464-10472, Dec. 1998.

[8] L. F. Abbott and S. B. Nelson, "Synaptic plasticity: Taming the beast," *Nat. Neurosci.*, vol. 3, pp. 1178-1183, Nov. 2000.

[9] G. Q. Bi and M. M. Poo, "Synaptic modification by correlated activity: Hebb's postulate revisited," *Annu. Rev. Neurosci.*, vol. 24, pp. 139–166, Mar. 2001.

[10] S. M. Bohte, J. N. Kok, and H. La Poutre, "Error-backpropagation in temporally encoded networks of spiking neurons," *Neurocomputing*, vol. 48, no. 1, pp. 17 - 37, 2002.

[11] R. Guyonneau, R. VanRullen, and S. J. Thorpe, "Neurons tune to the earliest spikes through STDP," *Neural Comput.*, vol. 17, no. 4, pp. 859-879, Apr. 2005.

[12] R. Gütig and H. Sompolinsky, "The tempotron: A neuron that learns spike timing-based decisions," *Nat. Neurosci.*, vol. 9, no. 3, pp. 420–428, Feb. 2006.

[13] T. Masquelier and S. J. Thorpe, "Unsupervised learning of visual features through spike timing dependent plasticity," *PLoS Comput. Biol.*, vol. 3, no. 2, p. e31, 2007.

[14] T. Masquelier, R. Guyonneau, and S. J. Thorpe, "Spike timing dependent plasticity finds the start of repeating patterns in continuous spike trains," *PloS one*, vol. 3, no. 1, pp. e1377, Jan. 2008.

[15] T.Masquelier, R. Guyonneau, and S. J. Thorpe, "Competitive STDP-based spike pattern learning," *Neural Comput.*, vol. 21, no. 5, pp. 1259-1276, Apr. 2009.

[16] F. Ponulak and A. Kasi´nski, "Supervised learning in spiking neural networks with ReSuMe: Sequence learning, classification, and spike shifting." *Neural Comput.*, vol. 22, no. 2, pp. 467-510, Feb. 2010.

[17] A. Mohemmed, S. Schliebs, S. Matsuda, and N. Kasabov, "Span: Spike pattern association neuron for learning spatiotemporal spike patterns," *Int. J. Neural Syst.*, vol. 22, no. 04, p. 1250012, 2012.

[18] J. Wang, A. Belatreche, L. Maguire, and T. M. McGinnity, "An online supervised learning method for spiking neural networks with adaptive structure," *Neurocomputing*, vol. 144, pp. 526 - 536, 2014.

[19] P. U. Diehl and M. Cook, "Unsupervised learning of digit recognition using spike-timing-dependent plasticity," *Front. Comput. Neurosci.*, vol. 9, no. 99, 2015.

[20] P. Ferré, F. Mamalet and S. J. Thorpe, "Unsupervised feature learning with winner-takes-all based STDP," *Front. Comput. Neurosci.*, vol. 12, Art. no. 24, Apr. 2018.

[21] S. R. Kheradpisheh, M. Ganjtabesh, S. J. Thorpe and T. Masquelier, "STDP-based spiking deep convolutional neural networks for object recognition," *Neural Netw.*, vol. 99, pp. 56-67, Mar. 2018.

[22] C. Mead, "Neuromorphic electronic systems," *Proc. IEEE*, vol. 78, no. 10, pp. 1629–1636, Oct. 1990.

[23] G. Indiveri, et al., "Neuromorphic silicon neuron circuits," *Front. Neurosci.*, vol. 5, Art. no.73, May 2011.

[24] F. Alibart, E. Zamanidoost, and D. B. Strukov, "Pattern classification by memristive crossbar circuits using ex situ and in situ training," *Nat. Commun.* vol. 4, Art. no. 2072 Jun. 2013.

[25] E. Painkras, et al., "Spinnaker: A 1-w 18-core system-on-chip for massively-parallel neural network simulation," *IEEE J. Solid-St. Circ.*, vol. 48, no. 8, pp. 1943–1953, May 2013.

[26] B. V. Benjamin, et al., "Neurogrid: A mixed-analog-digital multichip system for large-scale neural simulations," *Proc. IEEE*, vol. 102, no. 5, pp. 699-716, May 2014.

[27] S. B. Furber, F. Galluppi, S. Temple, and L. A. Plana, "The SpiNNaker project," *Proc. IEEE*, vol. 102, no. 5, pp. 652–665, May 2014.

[28] P. A. Merolla, et al., "A million spiking-neuron integrated circuit with a scalable communication network and interface," *Science* vol. 345, no. 6197, pp. 668–673, Aug. 2014.

[29] M. Prezioso, F. Merrikh-Bayat, B. D. Hoskins, G. C. Adam, K. K. Likharev and D. B. Strukov, "Training and operation of an integrated neuromorphic network based on metal-oxide memristors," *Nature*, vol. 521, pp. 61–64, May 2015.

[30] Burr, G. W. et al. "Experimental demonstration and tolerancing of a large-scale neural network (165 000 synapses) using phase-change memory as the synaptic weight element," *IEEE T. Electron Dev.*, vol. 62, no. 11, pp. 3498–3507 Jul. 2015.

[31] Park, S. et al. "Electronic system with memristive synapses for pattern recognition," *Sci. Rep.* vol. 5, Art. no. 10123, May 2015.

[32] N. Qiao, H. Mostafa, F. Corradi, M. Osswald, F. Stefanini, D. Sumislawska and G. Indiveri, "A reconfigurable on-line learning spiking neuromorphic processor comprising 256 neurons and 128K synapses," *Front. Neurosci.*, vol. 9, Art. no. 141, Apr. 2015.

[33] J. Shen, et al, "Darwin: a neuromorphic hardware co-processor based on spiking neural networks," *Sci. China Inform. Sci.*, vol.59, no.2, pp. 1-5, Feb. 2016.

[34] R. A. Nawrocki, R. M. Voyles and S. E. Shaheen, "A mini review of neuromorphic architectures and implementations," *IEEE T. Electron Dev.*, vol. 63, no. 10, pp. 3819-3829, Aug. 2016.

[35] C. D. Schuman, T. E. Potok, R. M. Patton, J. D. Birdwell, M. E. Dean, G. S. Rose and J. S. Plank, "A survey of neuromorphic computing and neural networks in hardware," arXiv preprint arXiv:1705.06963, 2017.

[36] Yao, P. et al. "Face classification using electronic synapses," *Nat. Commun.* vol. 8, Art. no. 15199, May, 2017.

[37] C. Li, et al, "Efficient and self-adaptive in-situ learning in multilayer memristor neural networks," *Nat. Commun.*, vol. 9, Art. no. 2385, Jun. 2018.

[38] I. Boybat, et al., "Neuromorphic computing with multi-memristive synapses," *Nat. Commun.* vol. 9, Art. no. 2514 Jun. 2018.

[39] A. Hurtado, I. D. Henning, and M. J. Adams, "Optical neuron using polarization switching in a 1550 nm-VCSEL," *Opt. Express*, vol. 18, no.24, pp. 25170–25176, Nov. 2010.

[40] W. Coomans, L. Gelens, S. Beri, J. Danckaert, and G. Van der Sande, "Solitary and coupled semiconductor ring lasers as optical spiking neurons," *Phys. Rev. E*, vol. 84, no.3, Sep. 2011, Art. no.036209.

[41] A. Hurtado, K. Schires, I. Henning, and M. Adams, "Investigation of vertical cavity surface emitting laser dynamics for neuromorphic photonic systems," *Appl. Phys. Lett.*, vol. 100, no. 10, pp. 103703-103703, Mar. 2012.

[42] T. Van Vaerenbergh, M. Fiers, P. Mechet, T. Spuesens, R. Kumar, G. Morthier, B. Schrauwen, J. Dambre, and P. Bienstman, "Cascadable excitability in microrings," *Opt. Express*, vol. 20, no.18, pp. 20292-20308, Aug. 2012.

[43] M. A. Nahmias, B. J. Shastri, A. N. Tait, and P. R. Prucnal, "A leaky integrate-and-fire laser neuron for ultrafast cognitive computing," *IEEE J. Sel. Top. Quantum Electron.*, vol. 19, no. 5, p. 1800212, Sept./Oct., 2013.

[44] F. Selmi, R. Braive, G. Beaudoin, I. Sagnes, R. Kuszelewicz, and S. Barbay, "Relative refractory period in an excitable semiconductor laser," *Phys. Rev. Lett.*, vol.112, no.18, Art. no.183902, May 2014.

[45] B. J. Shastri, M. A. Nahmias, A. N. Tait, A. W. Rodriguez, B. Wu, and P. R. Prucnal, "Spike processing with a graphene excitable laser," *Sci. Rep.*, vol. 6, Art. no.19126, Jan. 2016.

[46] B. Romeira, R. Avo, J. M. L. Figueiredo, S. Barland, and J. Javaloyes, "Regenerative memory in time-delayed neuromorphic photonic resonators," *Sci. Rep.*, vol. 6, Art. no. 19510, Jan. 2016.

[47] P. R. Prucnal, B. J. Shastri, T. F. de Lima, M. A. Nahmias, and A. N. Tait, "Recent progress in semiconductor excitable lasers for photonic spike processing," *Adv. Opt. Photon.*, vol. 8, no. 2, pp. 228-299, May. 2016.

[48] S. Y. Xiang, H. Zhang, X. X. Guo, J. F. Li, A. J. Wen, W. Pan, and Y. Hao, "Cascadable neuron-Like spiking dynamics in coupled VCSELs subject to orthogonally polarized optical pulse injection," *IEEE J. Sel. Top. Quantum Electron.*, vol. 23, no. 6, p. 1700207, Nov./Dec. 2017.

[49] T. Deng, J. Robertson, and A. Hurtado, "Controlled propagation of spiking dynamics in vertical-cavity surface-emitting lasers: towards

neuromorphic photonic networks," *IEEE J. Sel. Top. Quantum Electron.*, vol. 23, no. 6, Art. no. 1800408, Nov./Dec. 2017.

[50] Y. H. Zhang, S. Y. Xiang, J. K. Gong, X. X. Guo, A. J. Wen, and Y. Hao, "Spike encoding and storage properties in mutually coupled vertical-cavity surface-emitting lasers subject to optical pulse injection," *Appl. Opt.*, vol. 57, no. 7, pp. 1731-1737, 2018.

[51] S. Y. Xiang, Y. H. Zhang, X. X. Guo, A. J. Wen, and Y. Hao, "Photonic generation of neuron-like dynamics using VCSELs subject to double polarized optical injection," *J. Light. Technol.*, vol. 36, no. 19, pp. 4227-4234, Mar. 2018.

[52] Y. H. Zhang, S. Y. Xiang, X. X. Guo, A. J. Wen, and Y. Hao, "Polarization-resolved and polarization-multiplexed spike encoding properties in photonic neuron based on VCSEL-SA," *Sci. Rep.*, vol. 8, Art. no.16095, Oct. 2018.

[53] M. P. Fok, Y. Tian, D. Rosenbluth, and P. R. Prucnal, "Pulse lead/lag timing detection for adaptive feedback and control based on optical spike-timing-dependent plasticity," *Opt. Lett.*, vol. 38, no. 4, pp. 419-421, Feb. 2013.

[54] R. Toole and M. P. Fok, "Photonic implementation of a neuronal algorithm applicable towards angle of arrival detection and localization," *Opt. Exp.*, vol. 23, no. 12, pp. 16133-16141, Jun. 2015.

[55] Q. Ren, Y. Zhang, R. Wang, and J. Zhao, "Optical spike-timing-dependent plasticity with weight-dependent learning window and reward modulation," *Opt. Exp.*, vol. 23, no. 19, pp. 25247-25258, Sept. 2015.

[56] B. Gholipour, P. Bastock, C. Craig, K. Khan, D. Hewak, and C. Soci, "Amorphous metal-sulphide microfibers enable photonic synapses for brain-like computing," *Adv. Opt. Mater.*, vol. 5, no. 3, pp. 635-641, Jan. 2015.

[57] R. Toole, A. N. Tait, T. F. de Lima, A. N. Tait, B. J. Shastri, P. R. Prucnal, and M. P. Fok. "Photonic implementation of spike-timing-dependent plasticity and learning algorithms of biological neural systems," *J. Light. Technol.*, vol. 34, no. 2, pp. 470-476, Jan. 2016.

[58] Q. Li, Z. Wang, Y. Le, C. Sun, X. Song, and C. Wu, "Optical implementation of neural learning algorithms based on cross-gain modulation in a semiconductor optical amplifier," *Proc. SPIE*, vol. 10019, 2016.

[59] Z. Cheng, C. Ríos, W. H. P. Pernice, C. D. Wright and H. Bhaskaran, "On-chip photonic synapse," *Sci. Adv.*, vol. 3, no. 9, Art. no. e1700160, Sep 2017.

[60] A. Hurtado, I. D. Henning and M. J. Adams, "Effects of parallel and orthogonal polarization on nonlinear optical characteristics of a 1550 nm VCSOA," *Opt. Express*, vol. 15, no. 14, pp.9084-9089, Jul. 2007.

[61] M. D. Sánchez, P. Wen, M. Gross, and S. C. Esener, "Rate equations for modeling dispersive nonlinearity in Fabry-Perot semiconductor optical amplifiers," *Opt. Express*, vol.11, no. 21, pp. 2689-2696, Oct. 2003.

[62] A. Hurtado1, and M. J. Adams, "Two-wavelength switching with 1550 nm semiconductor laser amplifiers," *J. Opt. Netw.*, vol. 6, no. 5, pp. 434-441, May. 2007.

[63] S. Y. Xiang, J. K.Gong, Y.H. Zhang, X. X. Guo, A. Wen, and Y. Hao, "Numerical implementation of wavelength-dependent photonic spike timing dependent plasticity based on VCSOA," *IEEE J. Quantum Electron.*, vol. 54, no. 6, p. 8100107, Dec. 2018.

[64] M. J. Adams, J. V. Collins, and I. D. Henning, "Analysis of semiconductor laser optical amplifiers," *IEE Proc.*, vol. **132**, no.1, pp. 58–63, Feb. 1985.

[65] C. Tombling, T. Saitoh, and T. Mukai, "Performance predictions for vertical-cavity semiconductor laser amplifiers," *IEEE J. Quantum Electron.*, vol. 30, no. 11, pp. 2491–2499, Nov. 1994.

[66] J. Piprek, S. Bjorlin, and J. E. Bowers, "Design and analysis of vertical-cavity semiconductor optical amplifiers," *IEEE J. Quantum Electron*, vol. 37, no. 1, pp. 127-134, Jan. 2001.

[67] P. Royo, R. Koda, and L. A. Coldren, "Vertical cavity semiconductor optical amplifiers: comparison of Fabry–Pérot and rate equation approaches," *IEEE J. Quantum Electron.*, vol. 38, no. 3, pp. 279-284, Mar. 2002.

[68] V. Gauss, A. Hurtado, D. Jorgesen, M. J. Adams, S. Esener, "Static and dynamic analysis of an all-optical inverter based on a vertical cavity semiconductor optical amplifier (VCSOA)," *Opt. Commun.*, vol. 284, no.9, pp. 2345-2350, May. 2011.

[69] E. S. Bjorlin, B. Riou, P. Abraham, J. Piprek, Y. j. Chiu, K. A. Black, A. Keating and J. E. Bowers, "Long wavelength vertical-cavity semiconductor optical amplifiers," *IEEE J. Quantum Electron.*, vol. 37, no. 2, pp. 274-281, Feb. 2001.

[70] J. Robertson, T. Deng, J. Javaloyes, and A. Hurtado, "Controlled inhibition of spiking dynamics in VCSELs for neuromorphic photonics: theory and experiments," *Opt. Lett.*, vol. 42, no. 8, pp. 1560-1563, Apr. 2017.

[71] T. Deng, et al. "Stable Propagation of Inhibited Spiking Dynamics in Vertical-Cavity Surface-Emitting Lasers for Neuromorphic Photonic Networks," *IEEE Access*, vol. 6, pp. 67951-67958, Oct. 2018.

[72] T. W. Hughes, M. Minkov, Y. Shi and S. Fan, "Training of photonic neural networks through in situ backpropagation and gradient measurement," *Optica*, vol. 5 no. 7, pp. 864-871 Jul. 2018.

Shuiying Xiang was born in Ji'an, China, in 1986. She received the Ph.D. degree from Southwest Jiaotong University, Chengdu, China, in 2013.

She is currently Associate Professor with State Key Laboratory of Integrated Service Networks, Xidian University, Xi'an, China. She is the author or coauthor of more than 80 research papers. Her research interests include neuromorphic photonic systems, brain-inspired information processing, spiking neural network, vertical cavity surface-emitting lasers, and semiconductor lasers dynamics.

Yahui Zhang was born in Zhangjiakou, China, in 1993. She is currently working toward the Ph.D. degree from Xidian University, Xi'an, China. Her researching interest is the vertical cavity surface-emitting lasers, neuromorphic photonic systems, brain-inspired information processing, spiking neural network,

Junkai Gong was born in Yulin, China, in 1993. He is currently working toward the M.S. degree from Xidian University, Xi'an, China. His researching interest is the photonic spiking neural network and optical STDP.

Xingxing Guo was born in Ji'an , China, in 1993. She is currently working toward the M.S. degree from Xidian University, Xi'an, China. Her researching interest is the dynamics and applications of semiconductor lasers.

Lin Lin was born in Xi'an, China, in 1983. He received the Ph.D. degree from Xidian University, Xi'an, China in 2012.

He is currently a Lecturer at the School of Telecommunication Engineering, Xidian University. His current research interests the photonic spiking neural network and optical STDP.

Yue Hao was born in the city of Chongqing, China, in 1958. He received the Ph.D. degree from Xi'an Jiao tong University, Xi'an, China, in 1991.

He is currently a Professor at State Key Discipline Laboratory of Wide Bandgap Semiconductor Technology, the School of Microelectronics, Xidian University, Xi'an, China. His research interests include wide forbidden band semiconductor materials and devices.